

Durham E-Theses

Development of nanoparticle catalysts and total internal reflection (TIR) Raman spectroscopy for improved understanding of heterogeneous catalysis

BINGHAM, LAURA, MARIA

How to cite:

BINGHAM, LAURA, MARIA (2017) *Development of nanoparticle catalysts and total internal reflection (TIR) Raman spectroscopy for improved understanding of heterogeneous catalysis*, Durham theses, Durham University. Available at Durham E-Theses Online: <http://etheses.dur.ac.uk/12445/>

Use policy

The full-text may be used and/or reproduced, and given to third parties in any format or medium, without prior permission or charge, for personal research or study, educational, or not-for-profit purposes provided that:

- a full bibliographic reference is made to the original source
- a [link](#) is made to the metadata record in Durham E-Theses
- the full-text is not changed in any way

The full-text must not be sold in any format or medium without the formal permission of the copyright holders.

Please consult the [full Durham E-Theses policy](#) for further details.

Chapter 6. Catalytic applications of supported nanoparticle systems

A number of different nanoparticle systems have been synthesised, and both the synthesis and spectroscopic evaluation of these materials explored. Throughout this thesis the focus has been to bring together nanoparticles and spectroscopy with a long term goal of exploiting them for catalysis, by improving our understanding of catalytic mechanisms with new structural or spectroscopic insights. Although the focus in the long term is that these should be combined to study catalysis, in the course of conducting this work, a number of the nanoparticles developed were used solely because of their controlled structure to address questions above. Catalysis, and selected examples of this are shown in this chapter. This both demonstrates their utility in their own right, but possibly more importantly reinforces the idea that the materials and approach developed in this project, for studying catalysis using copper and other nanoparticle systems with TIR Raman spectroscopy, are amenable to use with real catalytic reactions.

6.1. Silver nanoparticles for amide bond synthesis, kinetics and reaction data

6.1.1. Catalytic testing of the reaction of two differing amines with benzyl alcohol for the direct creation of an amide bond

The formation of amide bonds is an area of significant interest due to their widespread use in organic chemistry and in biomedical applications.^{1,2} In the latter, where materials or compounds are used in humans, the prevalence of amide species in enzymes and proteins found within the body leads to a lowered risk of rejection. A simple high yielding, atom efficient process capable of forming amide bonds directly from alcohols and amines does not currently exist. Furthermore the generation of waste is a key issue with common synthesis techniques, such as those using activated acid derivatives (such as acid chlorides), or rearrangement reactions induced by an acid or a base, producing toxic waste.^{3,4} A variety of differing approaches have been put forward including synthesis with transition metal catalysts *via* nitriles,⁵ oximes,⁶ and aminocarbonylation.⁷ One approach that has gained significant interest is that of the reaction of terminal alkynes with sulfonyl azides in the presence of a copper(I) catalyst.⁸⁻¹⁰ Groups such as Milstein *et al.* believed that, unlike these methods which are atom inefficient and go *via* intermediate species, direct catalytic reaction of alcohols and amines to produce amides could take place with only dihydrogen released as a side product.⁹ This is desirable due to the high atom efficiency achieved, along with the absence of activating agents and the lack of waste products generated. Furthermore, it

allows for a catalogue of amides to be synthesised from a range of simple substrates. In the work of Milstein *et al.* a homogeneous ruthenium catalyst with a dearomatized 2-(di-tert-butylphosphinomethyl)-6-(diethylaminomethyl)pyridine) (PNN) type ligand was used. No acidic or basic promoter was required.¹¹

The direct acylation of amines was achieved through equimolar reaction with alcohols. The resulting formation of amides and molecular hydrogen took place with high yields and turnover numbers (TON) – refluxing (6 h) in toluene in a closed system gave a 63% yield, although longer (40 h) reaction resulted in a mixture of products. However, it was then found that flushing with argon flow, throughout the reaction to remove the hydrogen, took the same reaction (forming the amide benzylhexanamide) up to 96% yield, with only trace amounts of N-benzyl-hexyl-1-amine (1%) recorded. A variety of variables were also explored such as the nature of the amine and alcohol groups. Exploration of the primary amines benzylamine, pentylamine, and cyclo hexylamine gave rise to methoxy-acetylated amides in high yields (99, 78, and 99% respectively). The use of diamines was explored with high (88%) yields being recorded without the need for additional protecting agents.

Two possible pathways for the reaction were put forward (Figure 6.1 top scheme, labelled as pathways a, and b respectively). Firstly that dehydrogenation of the alcohol leads to aldehyde formation with subsequent reaction with a primary amine yielding the hemiaminal. The dehydrogenation of this hemiaminal then leads to formation of the amide. The second mechanism proposed was that of hemiacetal formation from the aldehyde and alcohol, followed by dehydrogenation to give an ester. Reaction of the ester with the amine leads to the formation of the amide. Given that running the reaction of hexyl hexanoate with benzylamine at reflux for 8 hours (under argon) both in the presence and absence of the catalyst did not produce N-benzylhexanamide the second proposed pathway was ruled out. It was, therefore, likely that the reaction goes *via* the hemiaminal pathway (pathway a). The mechanism put forward for this reaction is given (Figure 6.1 bottom scheme) and was derived from the known behaviour of other pincer type complexes.^{11–13} A catalytic cycle leads to alcohol dehydrogenation giving aldehyde formation. Subsequent reaction with the amine leads to the formation of the hemiaminal, which reacts with complex 1 to give complex C. β -hydride elimination of complex C then leads to formation of the amide with generation of complex 2. Completion of the catalytic cycle takes place *via* elimination of dihydrogen from the complex.

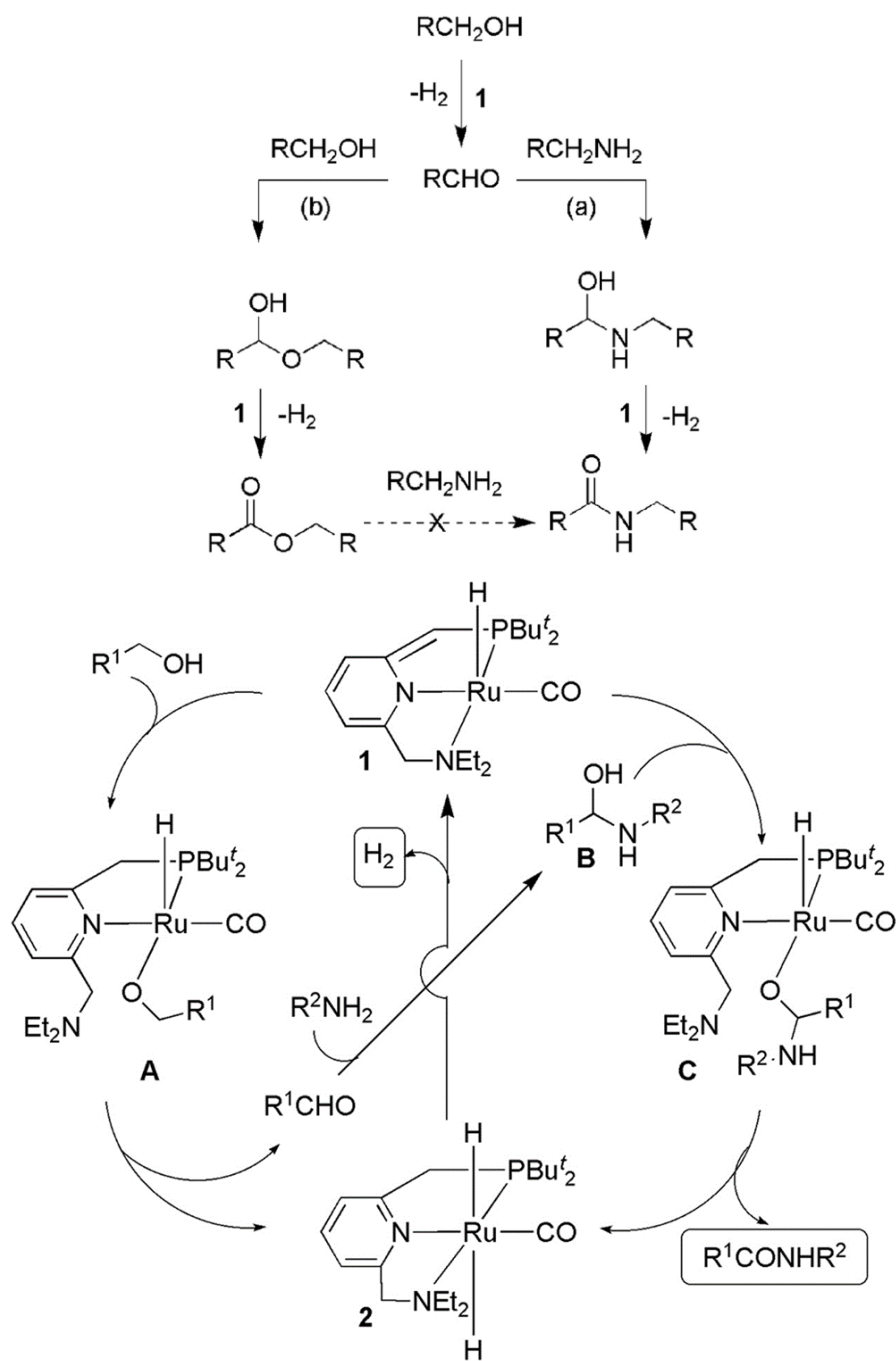


Figure 6.1. Scheme to show two proposed reaction pathways (top), and mechanism for the proposed reaction pathway (bottom). From Gunanathan, C.; Ben-David, Y.; Milstein, D. *Direct Synthesis of Amides from Alcohols and Amines with Liberation of H_2* . *Science* 2007, 317 (5839), 790–792. Reprinted with permission from AAAS.

Despite the advances made in the work of Milstein *et al.* and the subsequent work of others, in direct amidation from amines and alcohols, several notable disadvantages exist.^{9,14–19} Firstly, the catalyst does not tolerate secondary amines, secondly the homogeneous nature of the catalyst can make separation of catalyst from product challenging. To address the latter it is desirable to design a heterogeneous catalyst for this reaction. Satsuma *et al.* proposed that such a catalyst could be synthesised using a supported silver nanoparticle

system.²⁰ As has been discussed in Chapter 1, Section 1.6.4 silver nanoparticles are used within a variety of catalytic applications with their low cost (compared to precious metals) making them particularly desirable. As has been discussed extensively within this thesis nanoparticles display a variety of unique properties in catalysis compared to bulk materials with many catalysts containing nano-size metal particles, which often display high catalytic activity.²¹⁻²⁴ Although in the present thesis the focus has been to prepare nanoparticles of a well-defined size, the catalyst proposed contained nano-size silver particles prepared by impregnation of silver nitrate onto a suitable support material. Subsequent drying, and calcination and reduction of the support, and specifically the temperature at which reduction occurs was thought to control the particle size seen. The authors optimised conditions were used as a starting point within our work, 5 wt.% silver on alumina in the presence of caesium carbonate base giving the highest yield from many different transition metals, loadings, supports and bases tested. Since strong basic or acidic supports did not produce the same high yields the authors suggested such reactivity may be related to the availability of both acidic and basic sites at the alumina support surface. They reported a precedent for this behaviour in their prior work on alcohol dehydrogenation in the absence of an oxidant.²⁵ Reflux conditions were chosen with reaction yields increasing as the reaction temperature was increased upwards from 100 °C. A 1:2 molar ratio of alcohol to amine was seen to result in the highest product yield (91% under their reaction conditions). Furthermore, under these optimised conditions successful reaction was seen with secondary amines. In order to exclude any contribution from a homogeneous catalyst from leaching of the silver the reaction was stopped and the catalyst removed (by centrifugation). Further continuation of the reaction in the absence of the heterogeneous catalyst for an extended time period (22 h) did not produce any amide.

The authors proposed the mechanism shown in Figure 6.2 based upon that for direct amidation *via* the homogenous ruthenium catalyst above.

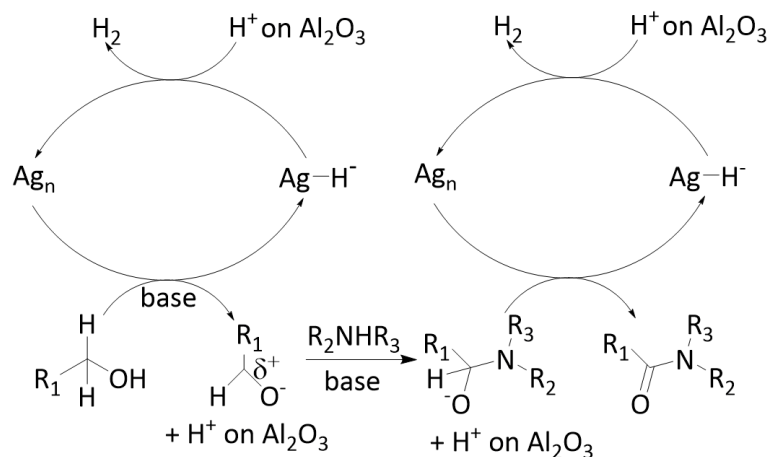


Figure 6.2. Scheme to show the mechanism proposed for direct amide formation from an amine and an alcohol over a silver nanoparticle based heterogeneous catalyst. Reproduced from Shimizu, K.; Ohshima, K.; Satsuma, A. Direct Dehydrogenative Amide Synthesis from Alcohols and Amines Catalyzed by γ -Alumina Supported Silver Cluster. *Chem. - Eur. J.* 2009, 15 (39), 9977–9980. Reprinted with permission from Wiley.

Parameters explored by the authors (under the optimised conditions) in order to obtain mechanistic insight include the variation of the nature of benzyl alcohol with electron donating and withdrawing groups, and exploration of particle size. For the substituents reactivity could be modelled using a Brown–Okamoto parameter and the resulting plot suggested that:

“a transition state of the rate-determining step involves a positive charge at α -carbon atom adjacent to the phenyl ring.”

From this the authors concluded that the rate determining step in the reaction was the C-H cleavage by the silver catalyst in either the alkoxide or hemi-aminal species. An exploration of particle size (by varying metal loading) showed higher TONs resulted, particularly from those with an average particle diameter below 2 nm, which have a high fraction of corner silver atoms.²⁶ This led the authors to conclude these sites are crucial to the reaction and required for the rate-determining step (C-H cleavage). However, it should be noted that the dispersity of the particle size distributions were not provided. Methodologies developed within this thesis for the synthesis of silver nanoparticles with a small controllable particle size could therefore be proposed to give improved catalytic activity or an improved test of how important the size effect is (the particles being produced here being consistently larger than the 2 nm they report to be crucial for the high rates observed).

Two example reactions of this class and that are selected for use in this work are given below (Figure 6.3 A and B). In the simplest case (Figure 6.3 A), as explored by Satsuma *et al.*,²⁰ reaction with piperidine can only lead only to formation of one product whichever reaction route (marked as path 1, and 2 in Figure 6.3 A) is taken. In the case of reaction with benzylamine (Figure 6.3 B) differing products can result from the differing reaction pathways (marked as paths 1-4 in Figure 6.3 B). This allows discrimination of which route or routes is/are taken. The section below details the study of both catalytic routes using a variety of silver catalysts synthesised from adaptation of the work of Satsuma *et al.*²⁰ Preliminary work by a MChem student (Harriet Barker, HB) using catalysts synthesised based on various adaptations of Satsuma's method (for the scheme given in Figure 6.3 A) suggested low activities for most of the catalysts tested. Directly following Satsuma's synthesis, calcination and reduction protocol, specifically calcining the catalyst in air to oxidise the silver and then reducing in hydrogen only for a very short period of time (typically 10 min), gave rise to a catalyst which had an exceptionally high activity, comparable to that seen by Satsuma *et al.* Of the various bases tried caesium carbonate was found to give the highest conversions to *N*-benzoylpiperidine, likely due to its greater solubility in the reaction medium. Further unpublished results indicated for the reaction of benzyl alcohol and benzylamine (Figure 6.3 B) the catalyst support is crucial with ceria only producing amide whilst other supports formed the undesired product *via* the imine.²⁷ This might suggest that in the work of Satsuma where they used ceria, magnesium oxide, zirconium dioxide, alumina, and silica supports that the imine formed, as a result of formation of the aldehyde and subsequent reaction with the amine. In the work conducted by the Aston group sodium methoxide was reported to be the optimal base, which is again highly soluble in the reaction medium. The section below details the study of both primary and secondary amine reagents using a variety of silver catalysts synthesised from adaptation of the work of Satsuma *et al.*²⁰

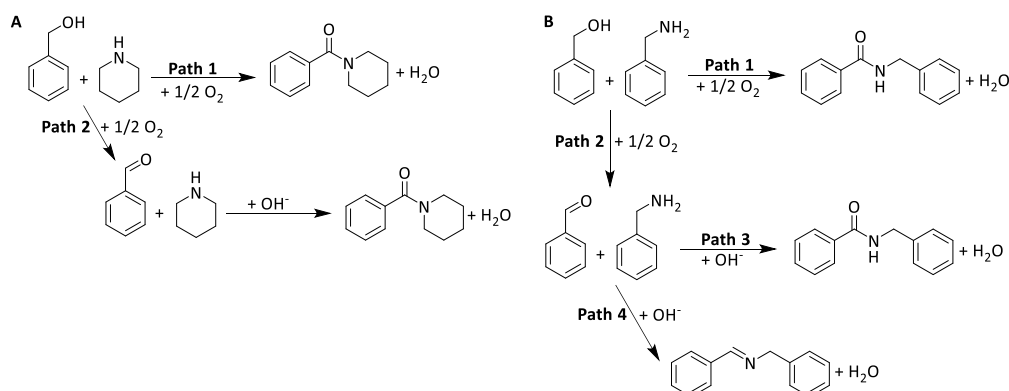
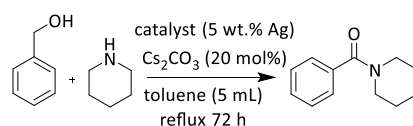


Figure 6.3. Reaction schemes for the reaction of benzyl alcohol with A) piperidine and B) benzylamine.

For each reaction both caesium carbonate and sodium methoxide bases were tested (Tables 6.1-6.4). Following preliminary work by HB the solvent volume was increased from 2 to 5 mL in order to provide a larger reaction volume, and the reaction was extended from the 24 h used by Satsuma *et al.* to 72 h to ensure the reaction had reached completion. It should be noted that the detection limit of the gas chromatography (GC) spectrometer was 0.1 μ V min. Furthermore typical errors received for repeats of the completed reaction with analysis by GC had been determined by previous members of the group to be in the range 2-3% of the value obtained. Correspondingly results have been shown to 1.d.p. Product yields were calculated from the GC trace using a methylnaphthalene internal standard (with use of response factors as described within the Appendix), from a starting concentration of 1 mmol methylnaphthalene, where the only product seen was N-benzoylpiperidine. A series of catalysts were used to explore the effect of reduction and oxidation upon the catalytic conversion seen. A preliminary experimental run showed broadly similar results to those about to be reported, but did not contain an internal standard and so is not discussed further as quantitative results were not obtained. Catalysts calcined (at 600 °C for 1 h under flow of nitrogen and oxygen, see Chapter 2, Section 2.2.6.2) but with no further reduction step showed either no or low catalytic conversion across all three of the reaction conditions trialled (the second reaction conditions, shown in Table 6.2 were not trialled, but could be included in extension of this project). Satsuma *et al.* utilised a 10 min reduction period (with reduction at 300 °C under a 50:50 flow of nitrogen:hydrogen) and obtained a 82% yield under identical conditions to those in the following tables, apart from the lower solvent volume and shorter 24 h reaction period described above.²⁰ It should be noted that for the short 10 min reduction period nitrogen was first purged through the line and all pipework (for 1 h prior to the reaction) in order to ensure hydrogen was delivered immediately. Initial use of the parent catalyst prepared using this short (10 min) reduction period, for the reaction of piperidine and benzyl alcohol with the caesium carbonate base, showed a small conversion to N-benzoylpiperidine. This value was orders of magnitude smaller than that recorded by Satsuma *et al.*²⁰ No product yield was seen with a longer 3 h reduction period for the catalyst with no product peak recorded in the GC trace (a 3 h reduction period was chosen to ensure the catalyst surface was fully reduced). The inability of both the unreduced and the 3 h reduced catalyst to provide any product conversion might be an indication of the very specific nature of the catalyst required. In the present case the catalyst was prepared using a similar support material to that used by Satsuma *et al.* (γ -alumina), however porosity or

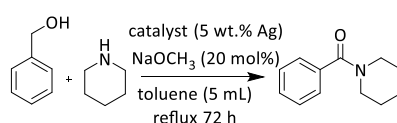
structure differences between batches may alter the impregnation process rendering the produced catalysts similar but not identical.

Table 6.1. Catalytic data for the reaction of benzyl alcohol and piperidine (1:2 molar ratio) over a silver/alumina (Ag/Al₂O₃) catalyst with a caesium carbonate (Cs₂CO₃) base. Catalysts were prepared and reactions were undertaken according to Satsuma *et al.*²⁰ It should be noted that an increased solvent volume and increased reaction time of 5 mL and 72 h was employed versus the original 2 mL and 24 h used by Satsuma *et al.*²⁰ These changes were made in order to give a sufficiently large reaction volume and to ensure completion of the reaction. All catalysts were calcined under a nitrogen flow (12.5 mL min⁻¹) at 600 °C for 1 h (see Section 2.2.6.2.2). All reductions (when performed) took place at 300 °C under a flow of nitrogen (12.5 mL min⁻¹) and hydrogen (12.5 mL min⁻¹). For the short 10 min reduction period hydrogen was purged through the all interconnecting gas tubing for 1 h prior to the flow of nitrogen for calcination, this was to ensure the immediate addition of hydrogen during the short 10 min reduction period. Product yields were calculated from the GC trace using a methylnaphthalene internal standard (with use of response factors as described within the Appendix), from a starting concentration of 1 mmol methylnaphthalene, where the only product seen was N-benzoylpiperidine. Gas chromatography – mass spectrometry (GCMS): It can be noted that both polar and non-polar columns were used for GCMS to ensure no product or reagent species went un-detected. *Catalytic data from the 10 min reduction of catalyst prepared by the satsuma method by HB, under the typical conditions stated above.



Sample	Product yield / %
Ag / Al ₂ O ₃ Satsuma method- not reduced	0
Ag / Al ₂ O ₃ Satsuma method- 10 min reduced	0.2
Ag / Al ₂ O ₃ Satsuma method- 10 min reduced*	0
Ag / Al ₂ O ₃ Satsuma method- 3 h reduced	0

Table 6.2. Catalytic data for reaction of benzyl alcohol and piperidine (1:2 molar ratio) over a silver/alumina (Ag/Al₂O₃) catalyst with a sodium methoxide (NaOCH₃) base. Catalysts were prepared and reactions were undertaken according to Satsuma *et al.*²⁰ It should be noted that an increased solvent volume and increased reaction time of 5 mL and 72 h was employed versus the original 2 mL and 24 h used by Satsuma *et al.*²⁰ These changes were made in order to give a sufficiently large reaction volume and to ensure completion of the reaction. All catalysts were calcined under nitrogen (12.5 mL min⁻¹) at 600 °C for 1 h (see Section 2.2.6.2.2). All reductions took place at 300 °C under a gas flow of nitrogen (12.5 mL min⁻¹) and hydrogen (12.5 mL min⁻¹). For the short 10 min reduction hydrogen was ran through the all interconnecting gas tubing for 1 h prior to the flow of nitrogen for calcination, this was to ensure the immediate addition of hydrogen during the short 10 min reduction period. Product yields were calculated from the GC trace using a methyl-naphthalene internal standard (with use of response factors as described within the Appendix), from a starting concentration of 1 mmol methyl-naphthalene, where the only product seen was N-benzoylpiperidine. GCMS: It can be noted that both polar and non-polar columns were used for GCMS to ensure no product or reagent species went un-detected *Catalytic data from the 10 min reduction of catalyst prepared by the satsuma method by HB, under the typical conditions stated above.



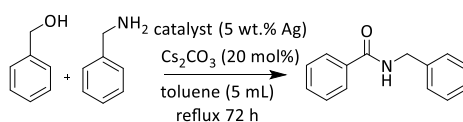
Sample	Product yield / %
Ag / Al ₂ O ₃ Satsuma method- 10 min reduced*	0
Ag / Al ₂ O ₃ Satsuma method- 3 h reduced	0

For the reaction of benzyl alcohol and benzylamine (Tables 6.3, and 6.4) conversion to *N*-benzylidene benzylamide (the product formed *via* the imine) was seen in all cases. An exemplar spectra of the GC trace showing its appearance is given in Figure 6.4 for the sample labelled “Ag / Al₂O₃ satsuma method-10 min reduced*” in Table 6.4. Use of the 3 h reduction period gave comparable results for reaction with caesium carbonate to that seen for the 3 h reaction with sodium methoxide, although a very slight increase in yield was seen with the caesium carbonate. Satsuma *et al.*,²⁰ had reported that bases including carbonates were seen to give higher product yields than even strong bases such as sodium methoxide, although as noted the increase seen here was very small (in line with the small product yields seen). It is perhaps notable that we do not see any enamine or aldehyde formation which would be expected from this route (*e.g.* if path 4 in Figure 6.3 B is followed). Further work is needed to explore this fully, but as the present goal was to investigate if the silver nanoparticles prepared in Chapter 3 could be used as catalysts for this reaction, this was not pursued.

As stated above, the prior work of HB for the reaction of benzyl alcohol and piperidine following exactly Satsuma's protocol had given rise to a 76% product yield for the reaction of piperidine and benzyl alcohol (given the different catalyst support and possibly experimental variations, comparable to the 82% reported by Satsuma *et al.*).²⁰ In order to explore if the low or negligible conversions now seen in fresh preparations of these catalysts in this project were a function of the catalysts' syntheses, one of HB's original catalysts (which had given rise to product conversion) was calcined and reduced according to the conditions specified above (calcined under nitrogen 12.5 mL min⁻¹ at 600 °C for 1 h, see Section 2.2.6.2.2), and reductions took place at 300 °C under a gas flow of nitrogen (12.5 mL min⁻¹) and hydrogen (12.5 mL min⁻¹), and used for all four catalyst runs (Tables 6.1-6.4, starred results). In the case of the reaction of piperidine and benzyl alcohol no conversion was seen. For reaction with benzylamine the highest conversions reported for each series were seen (Tables 6.3-6.4) with this catalyst, with the use of sodium hydroxide base giving the highest overall conversion. The conversion values seen in these experiments are still much lower than those reported by Satsuma *et al.*,²⁰ however, the reasons for this are unclear, although most likely attributable to the difficulty in reproducing exactly the right oxidation state of the surface. This was not really considered in the original study and the metallic nature of the silver was only confirmed by EXAFS after 30 mins of reduction, whereas their active 10 min reduced catalyst was not characterised in this way.²⁵ No data was presented to suggest that only metallic silver was present after the shorter reduction period.

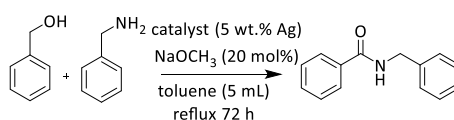
As emphasized above, the goal of the present study was to identify whether our previously prepared silver nanoparticles could be employed for studying this catalytic system. Furthermore, identifying a nanoparticle system that could be used in future studies could enable the oxidation state questions to be addressed in a number of ways. For instance, surface oxides are known to exist at the surface of these nanoparticle systems and these surface oxides could be a means of delivering and investigating the effect of small quantities of surface localised oxides on a suitable silver based catalyst.²⁰ Metal support interactions are also known to generate M⁺ sites at the metal-metal oxide interface.²⁸ However, as optimisation of this brief 10 min reduction protocol was problematic, for the initial study of the nanoparticle system a different approach was taken and in the first instance the catalysts were always reduced for a longer period so more stable structures would be generated. Results for these silver nanoparticle catalysts for a variety of support systems are explored in the section below.

Table 6.3. Catalytic data for reaction of benzyl alcohol and benzylamine (1:2 molar ratio) over a silver/alumina (Ag/Al₂O₃) catalyst with a caesium carbonate (Cs₂CO₃) base. Catalysts were prepared and reactions were undertaken according to Satsuma *et al.*²⁰ It should be noted that an increased solvent volume and increased reaction time of 5 mL and 72 h was employed versus the original 2 mL and 24 h used by Satsuma *et al.*²⁰ These changes were made in order to give a sufficiently large reaction volume and to ensure completion of the reaction. All catalyst were calcined under nitrogen (12.5 mL min⁻¹) at 600 °C for 1 h (see Section 2.2.6.2.2). All reductions took place at 300 °C under a gas flow of nitrogen (12.5 mL min⁻¹) and hydrogen (12.5 mL min⁻¹). For the short 10 min reduction hydrogen was ran through the all interconnecting gas tubing for 1 h prior to the flow of nitrogen for calcination, this was to ensure the immediate addition of hydrogen during the short 10 min reduction period. Product yields were calculated from the GC trace using a methyl-naphthalene internal standard (with use of response factors as described within the Appendix), from a starting concentration of 1 mmol methyl-naphthalene, where the only product seen was benzylidene benzylamide. Assignments were made using the GC standards (Section 2.2.6.2.4) with the exception of benzaldehyde and benzylidene benzylamine which were assigned using GCMS. It can be noted that both polar and non-polar columns were used for GCMS to ensure no product or reagent species went un-detected *Catalytic data from the 10 min reduction of catalyst prepared by the satsuma method by HB, under the typical conditions stated above.



Sample	Product yield / %
Ag / Al ₂ O ₃ Satsuma method- not reduced	0.7
Ag / Al ₂ O ₃ Satsuma method- 10 min reduced*	1.4
Ag / Al ₂ O ₃ Satsuma method- 3 h reduced	1.0

Table 6.4. Catalytic data for reaction of benzyl alcohol and benzylamine (1:2 molar ratio) over a silver/alumina (Ag/Al₂O₃) catalyst with a sodium methoxide (NaOCH₃) base. Catalysts were prepared and reactions were undertaken according to Satsuma *et al.*²⁰ It should be noted that an increased solvent volume and increased reaction time of 5 mL and 72 h was employed versus the original 2 mL and 24 h used by Satsuma *et al.*²⁰ These changes were made in order to give a sufficiently large reaction volume and to ensure completion of the reaction. All catalyst calcined under nitrogen (12.5 mL min⁻¹) at 600 °C for 1 h (see Section 2.2.6.2). All reductions took place at 300 °C under a gas flow of nitrogen (12.5 mL min⁻¹) and hydrogen (12.5 mL min⁻¹). For the short 10 min reduction hydrogen was ran through the all interconnecting gas tubing for 1 h prior to the flow of nitrogen for calcination, this was to ensure the immediate addition of hydrogen during the short 10 min reduction period. Product yields were calculated from the GC trace using a methylnaphthalene internal standard (with use of response factors as descried within the Appendix), from a starting concentration of 1 mmol methylnaphthalene, where the only product seen was benzylidene benzylamide. It can be noted that both polar and non-polar columns were used for GCMS to ensure no product or reagent species went un-detected. *Catalytic data from the 10 min reduction of catalyst prepared by the satsuma method by HB, under the typical conditions stated above.



Sample	Product yield / %
Ag / Al ₂ O ₃ Satsuma method- not reduced	0.8
Ag / Al ₂ O ₃ Satsuma method- 10 min reduced*	4.0
Ag / Al ₂ O ₃ Satsuma method- 3 h reduced	0.6

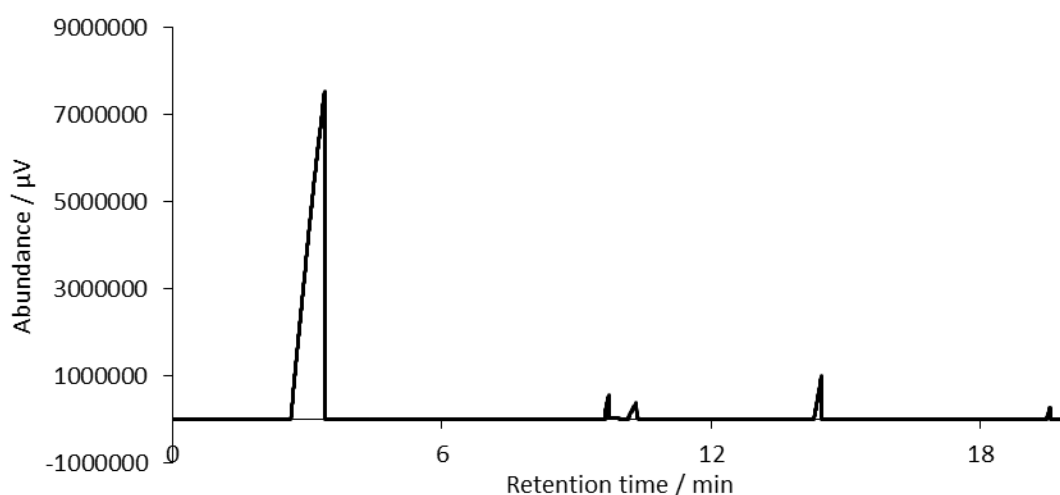


Figure 6.4. Exemplar GC spectra for "Ag / Al₂O₃ satsuma method-10 min reduced*" catalyst given in Table 6.4.

6.1.2. The investigation of silver nanoparticle catalysts for use in the direct formation of an amide bond from reaction of benzyl alcohol and piperidine

A variety of silver nanoparticle catalysts were synthesised and studied. Given that Satsuma *et al.* found that some of the lowest product yields were received for catalysts supported upon a cerium dioxide, or magnesium oxide support it was inferred that the properties of the support,²⁰ such as basicity, were important. Only the reaction of piperidine with benzyl alcohol was investigated in order to allow for simplification in the number of reactions run allowing for catalytic testing for a greater variety of support materials. BET (Brunauer–Emmett–Teller) and BJH (Barrett–Joyner–Halenda) values for the supports used were confirmed by co-workers in the group (HB) and were not repeated in this work. For the mesoporous silica support SBA-15 the BJH pore size diameter was 7.0 ± 1 nm, with a BET surface area of $950 \text{ m}^2 \text{ g}^{-1}$ and a pore volume of $2.5 \text{ cm}^3 \text{ g}^{-1}$ and a pore diameter of 9 nm as determined by nitrogen porosimetry. For KIT-6 (a different mesoporous silica support, see Section 2.1.7) BET characterisation gave a surface area of $40.9 \pm 0.2 \text{ m}^2 \text{ g}^{-1}$. X-ray diffraction (XRD) spectroscopy was also recorded for KIT-6 and is given in the Appendix (Figure 6A.1, and 6A.2). Nanoparticles were synthesised using a protocol I had developed from adaptation of Koski *et al.*,²⁹ (actual catalytic testing was undertaken by HB with supervision from me). It should be noted that all catalysts reported in this section were reduced for 30 min (unless otherwise stated), as opposed to the 10 min used in the section above and reported by Satsuma. This was in order to attempt full reduction of the silver which may not be achieved for shorter reduction times. It also, reduces the risk of slight variations in reduction time dramatically affecting catalyst performance, which seemed to be critically important for the Satsuma-type catalyst.

Transmission electron microscopy (TEM) images are shown (Figure 6.5) for silver/oleylamine/oleic acid nanoparticles (silver/OAm/OAc nps) synthesised with two differing ripening times. A tight particle size distribution was seen for the 2 min ripened nanoparticles centred around 6 nm (TEM data for the same nanoparticle batch was shown in Chapter 3, Section 3.1.2). However, for the 1 h ripened silver nanoparticles despite the particle size averaging at a similarly small value (around 5 nm) a minority of very large agglomerates were seen (Figure 6.5 B). The work shown here was carried out prior to some of the optimisation of the methods detailed in Chapter 3 and the particle size distribution for the 1 h ripened particles (Figure 6.5 A) was noticeably much larger than reported in Chapter 3, although this is unlikely to alter the conclusions of this section, in that the 1 h sample provides small and large particles whereas the 2 min sample contains only small particles.

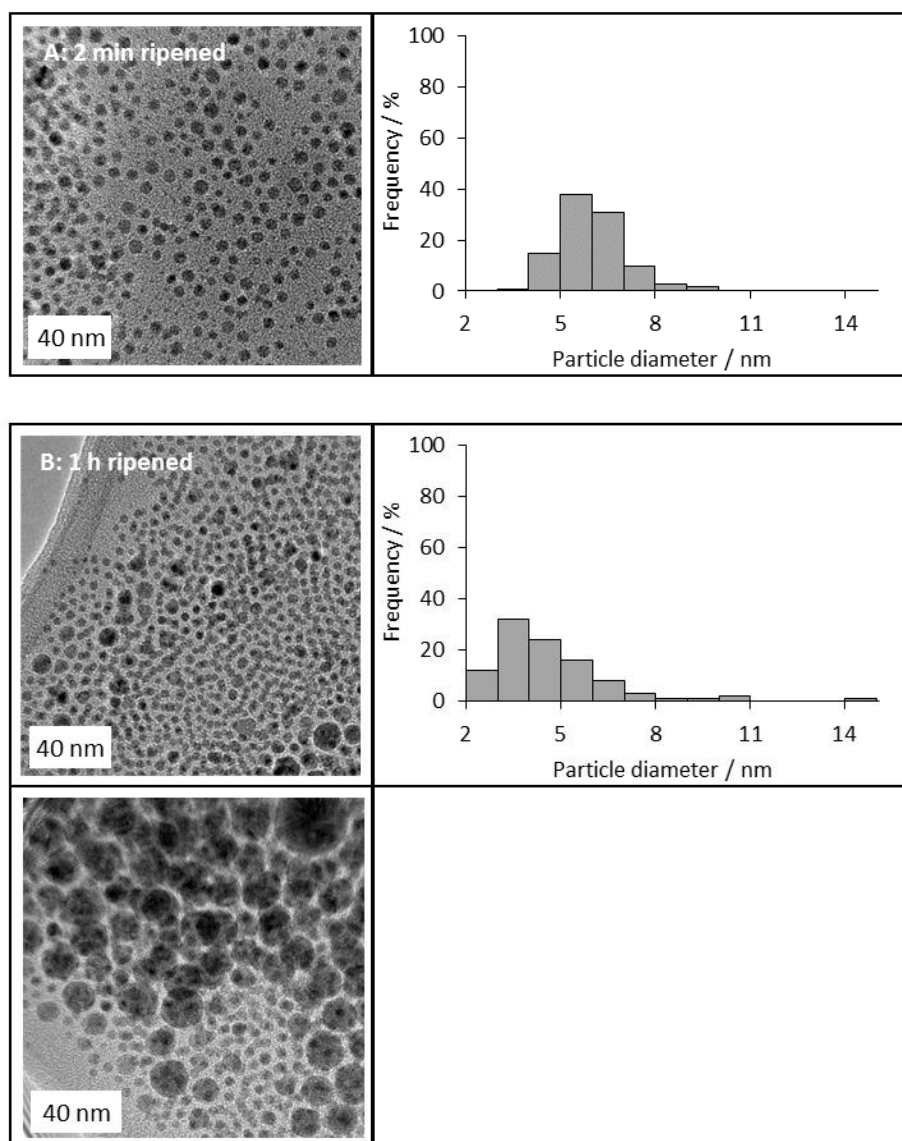


Figure 6.5. A) (left) Typical TEM image of as synthesised silver/OAm/OAc nps with 2 min ripening time (synthesised as outlined in Section 2.2.1.4), (right) Corresponding particle size distribution (6 ± 1 nm) obtained from multiple images of this sample. B) (left) Typical TEM image (top) and atypical aggregated area (bottom) for as synthesised silver/OAm/OAc nps with 1 h ripening time (synthesised as outlined in Section 2.2.1.4) (right) Corresponding particle size distribution (5 ± 2 nm) obtained from multiple images of this sample.

TEM data was also recorded for the supported nanoparticles (supported upon γ -alumina) as shown in Figure 6.6. Close inspection reveals that within the structure of the alumina some nanoparticles can be seen indicating successful deposition of the silver nanoparticle upon the support. The low number of nanoparticles seen in the supported state meant that particle size analysis was not possible and would likely discriminate against smaller particles. However, visual comparison of Figures 6.5 and 6.6 does not indicate any significant change in the particle size. Energy Dispersive X-ray (EDX) spectroscopy (Figure 6.7) taken by focusing upon one of these particles within the support matrix confirmed that both silver, aluminium,

and oxygen were present along with copper and carbon attributed to the TEM grid. The difference in the intensity of the silver band versus the aluminium signal in the two spectra (for the 2 min ripened versus the 1 h ripened sample) is likely to relate to whether large particles were present in the specific region probed and should not be taken as an indication of nanoparticle loading. Many more sampling spots would be required to elucidate this, but in the present study EDX was employed only qualitatively to verify the sample identity and ensure it was free of possible contamination.

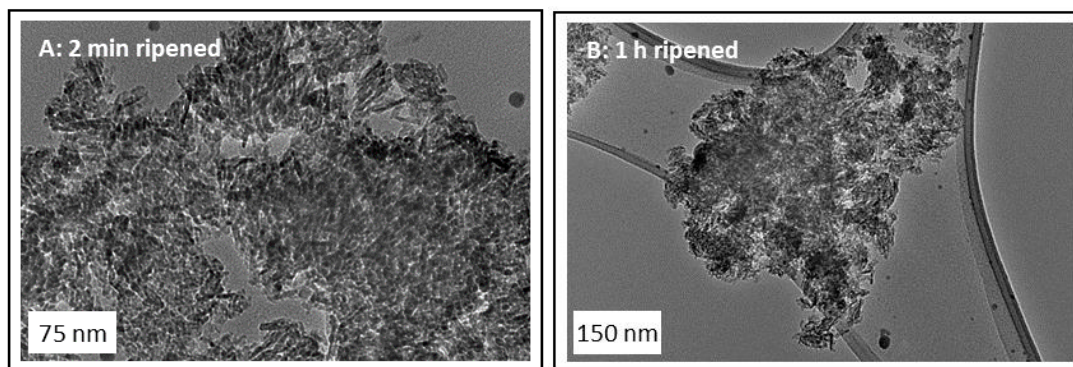


Figure 6.6. A) Typical TEM image of supported silver/OAm/OAc nps with a 2 min ripening time supported upon γ -alumina (synthesised and supported as outlined in Section 2.2.1.4 and 2.2.3.3) B) Typical TEM image for as synthesised silver/OAm/OAc nps with 1 h ripening time supported upon γ -alumina (synthesised and supported as outlined in Section 2.2.1.4 and 2.2.3.3).

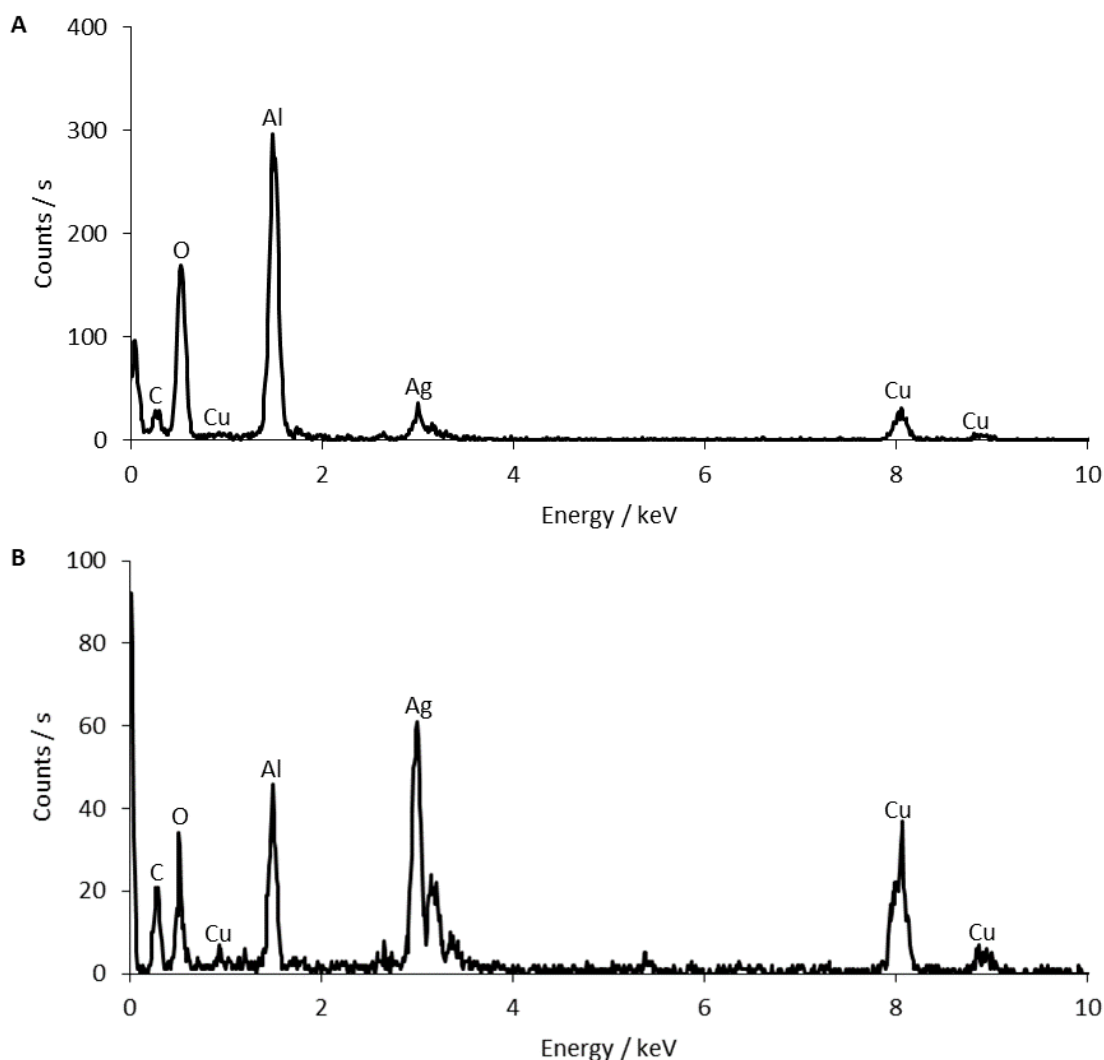
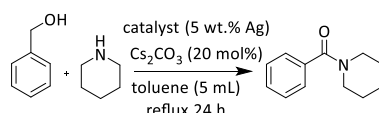


Figure 6.7. EDX chemical analysis taken for focusing upon the small circular particles within the support material for supported silver nanoparticles (synthesised and supported as outlined in Section 2.2.1.4 and 2.2.3.3) with a ripening time of A) 2 min and B) 1 h.

Catalytic testing (Table 6.5) revealed all catalysts showed significantly lower values of conversion than those reported by Satsuma *et al.*²⁰ Again Satsuma *et al* showed significantly higher values of conversion than for any other catalysts synthesised. However, in this case conversion was seen for the 1 h ripened silver catalyst supported on silica, cerium dioxide, and alumina. Satsuma and co-workers postulated the requirement for acidic and basic OH sites on the catalyst support and they believed these sites had an active role in the reaction mechanism. The γ -alumina supported catalyst would therefore be expected to give the highest product conversion given that it contains both acidic and basic OH sites. However, this was not the case for either of the two catalysts prepared. For the silica based support systems the low acidity and corresponding relative absence of acidic and basic OH sites was expected to result in low or no product conversion as seen. To investigate further the

requirement of acidic and basic sites, catalysts were synthesised with supports containing either predominantly basic or predominantly acidic sites. Silica (in the form of silica gel) contains only acidic OH sites and was chosen for supporting of the 1 h ripened silver nanoparticles. The wider range of pores sizes present in the gel was expected to be a more suitable match with the wider range of particle sizes present in the 1 h ripened sample. Conversely the cerium dioxide support system contained predominantly basic sites. For these two supports higher conversions relative to those on the alumina support are clearly seen, conversely to what was reported by Satsuma. Using nanoparticles which are identical (and not produced as a function of the support they are on as would be the case in the prior work by Satsuma), a different behaviour is seen, pointing to the fact that acidity/basicity alone is not the cause of any metal-support effect in this process. Finally, it is also notable that the nanoparticle catalysts on alumina only produced detectable product in the case of the 1 h ripened sample (containing large and small particles) and not the 2 min ripened sample that contained only small particles. This is inconsistent with the previously discussed hypothesis that small particles with many corner sites are crucial for the reaction.

Table 6.5. Catalytic data for reaction of benzyl alcohol and piperidine (1:2 molar ratio) with a caesium carbonate (Cs_2CO_3) base over various supported silver catalysts: silver/alumina ($\text{Ag} / \text{Al}_2\text{O}_3$), silver/OAm/OAc nps ($\text{Ag} \text{ np}$) with either 2 min or 1 h ripening times supported upon either alumina (Al_2O_3), SBA-15, silica gel (SiO_2), or cerium dioxide (CeO_2).¹⁸ Catalysts were prepared and reactions were undertaken according to Satsuma et al.,²⁰ with the value received by Satsuma et al. given in the first line of the table. It should be noted that an increased solvent volume and increased reaction time of 5 mL and 72 h was employed versus the original 2 mL and 24 h used by Satsuma et al..²⁰ These changes were made in order to give a sufficiently large reaction volume and to ensure completion of the reaction. All nanoparticle catalyst data was recorded by HB. All catalyst calcined under nitrogen (12.5 mL min^{-1}) at $600 \text{ }^\circ\text{C}$ for 1 h (see Section 2.2.6.2.2). All reductions took place at $300 \text{ }^\circ\text{C}$ under a gas flow of nitrogen (12.5 mL min^{-1}) and hydrogen (12.5 mL min^{-1}) for 30 mins, with the exception of Satsuma's catalyst which was reduced for 10 mins. Product yields were calculated from the GC trace using a dodecane internal standard (with use of response factors as described within the Appendix), where the only product seen was N-benzoylpiperidine.



Sample	Product yield / %
Ag/Al_2O_3 literature value-	82
Satsuma method	
2 min Ag np / Al_2O_3	0
1 h Ag np / Al_2O_3	1
2 min Ag np / SBA-15	0
1 h Ag np / SiO_2	14
1 h Ag np / Al_2O_3 oxidised only	50
1 h Ag np/ CeO_2	20

In conclusion, attempts to use a previously reported silver catalyst for direct amide bond synthesis identified that the achievable rate was extremely sensitive to oxidation state of the surface sample (or possibly other factors) and could not be reproduced reliably. It was, however, possible to employ the previously prepared silver nanoparticles as catalysts for this reaction – a proof of concept for further such studies using these nanoparticle systems. Furthermore, the nanoparticles enabled testing with a range of supports (without influence of the support on silver particle formation) to test the theory of acidity/basicity put forward previously, but again the results of this were clearly at odds with the previous literature study. Finally the conversion was seen to only occur when larger silver particles were

present, suggesting the hypothesis that corner sites of small < 2nm particles were crucial for catalysis to be incorrect.

6.2. Furfural hydrogenation using platinum and copper Single Atom Alloys (SAAs)

6.2.1. Introduction

The hydrogenation of furfural to furfural alcohol has been the source of much research due to the widespread use and chemical importance of the product. Furfural alcohol is an intermediate for a variety of products including plasticizers, lubricants, resins, and dispersing agents.³⁰⁻³² Copper chromite catalysts have been used widely as industrial catalysts for furfural hydrogenation with their success being particularly attributed to their ability to selectively hydrogenate carbonyl groups and not alkenes.^{33,34} Despite the reasonable activity and selectivity shown, the copper chromite catalyst and its disposal poses a significant threat to human health.^{35,36} Consequently, work has been undertaken to find a suitable replacement. A variety of precious metals (such as nickel, ruthenium, platinum, cobalt, copper) have been investigated as potential catalysts, with reactions trialled in both the vapour and liquid phase.^{32,37-40} Platinum catalysts in particular have emerged as a promising candidate for vapour phase furfural hydrogenation,⁴¹⁻⁴³ and a variety of factors including the support nature and particle size have been shown to be important.^{32,41,44,45} As touched upon above a key challenge is the catalysts selectivity. For example in the vapour phase a wide variety of products can be formed, including: furfuryl alcohol, 2-methylfuran, furan, tetrahydrofuran, tetrahydrofurfuryl alcohol, and products such as pentanols and pentanediols from ring decomposition.³⁴ Figure 6.8 summarises the differing pathways available leading to desirable and undesirable products, correspondingly selectivity is a paramount problem.⁴⁶

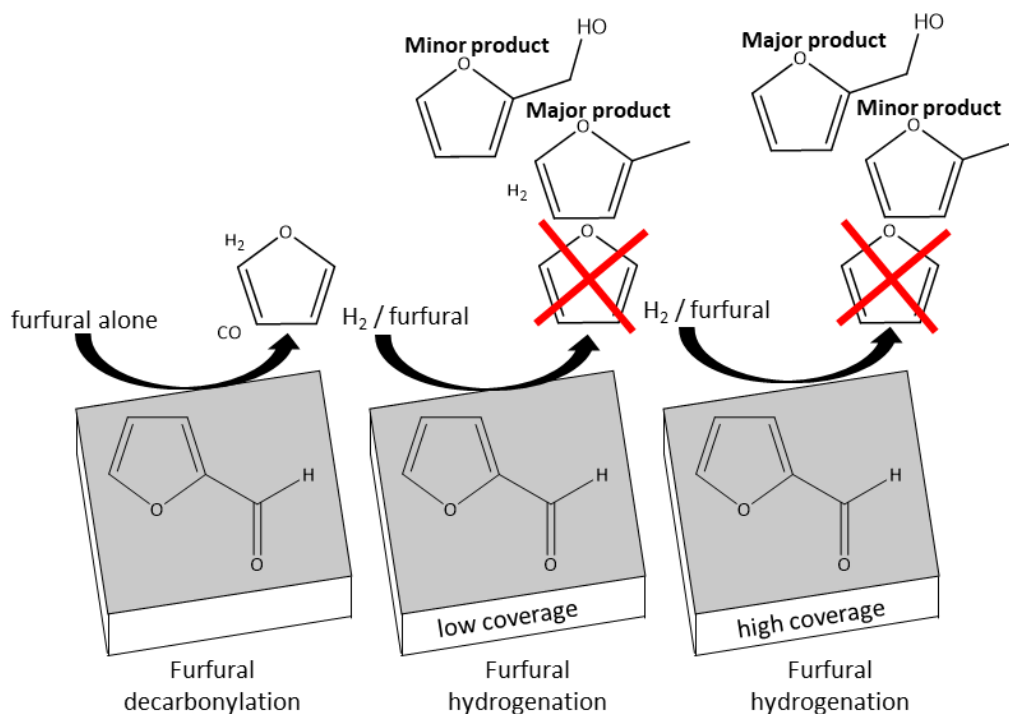


Figure 6.8. Reaction schemes to demonstrate selectivity issues faced in furfural hydrogenation.

The idea put forward by Kyriakou *et al.* in the field of hydrogenation in general but that we believe is applicable to furfural hydrogenation, was atomically dispersing a surface of the catalytically active metal onto a more inert support material, which was completely inactive for hydrogenation (in this case copper).^{47–50} The group were the first to find that, under UHV conditions, the addition of isolated palladium atoms to a copper surface, referred to as a Single Atom Alloy (SAA), gave differing catalytic properties to that of copper or palladium alone. This strategy was seen to achieve not only the desired cost reductions, but also to provide significant enhancements in reaction selectivity. In the context of a wider collaboration with Aston University I have taken the copper nanoparticle system developed in this work and doped sub-monolayer quantities of metals such as palladium or platinum onto the surface of the copper using a galvanic displacement approach.⁵¹ The reduction potential of Cu(II) is 0.34 V, and for Pt(II) is 1.2 V.⁵² Galvanic displacement is based on the redox process, where the copper surface is oxidized while the platinum (or palladium) is reduced, resulting in the incorporation of platinum at the copper surface. Catalytic testing of these materials (undertaken by Aston University) for furfural hydrogenation has shown enhancements in catalyst selectivity. By way of introduction, the following sub-sections review the prior work of Kyriakou *et al.*,^{47–50} which forms the basis of the work I have undertaken.

6.2.1.1. Early work of Single Atom Alloys (SAA), using low-temperature scanning tunnelling microscopy (LT-STM) and Density function theory (DFT) computational modelling

Initial understanding of these SAA type systems was gained through the use of Density Functional Theory (DFT) computational modelling and Low-Temperature Scanning Tunnelling Microscopy (LT-STM). The interaction of the SAA with hydrogen was probed.⁴⁷⁻⁴⁹ These studies were conducted under UHV conditions. As has been eluded to previously within this report, UHV conditions allow for simplification and often constitute a good starting point for a catalytic study. However, it was unclear how well these systems replicate catalyst behaviour under actual operating conditions.

The samples were prepared by addition of the palladium onto a pre-existing copper surface using resistive heating of a wound palladium wire. Preparation temperature was seen to play a role in determining where, upon the copper surface, the palladium was deposited. Therefore, one initial focus of their work was upon the placement of the palladium on the host surface, as studied by DFT modelling. Precise prediction of the movement of the palladium across the copper surface was made, and indicated that the palladium was bound strongly to the step edges remaining there during the subsequent reaction. Crucially comparison of the palladium only single-atom catalyst and the copper and palladium SAA indicated that the copper surface was inert to dissociation of the un-activated hydrogen. This was due to the significant dissociation barrier present (0.34 eV). However, when palladium atoms were present at the catalyst surface the catalyst was active to hydrogen uptake, as well as to the subsequent dissociation, which leads to spillover onto the copper surface. Some precedent existed for this behaviour with similar effects, in terms of hydrogen activation and spill over, having been reported in the literature (for a titanium doped aluminium surface, and a silver doped gold surface respectively).^{53,54} Furthermore, the use of LT-STM allowed for the visualisation of this hydrogen spill over. They claimed this was possible due to the lowering of the electron tunnelling of the hydrogen through the hydrogen-palladium complex compared to palladium alone.^{55,56}

6.2.1.2. Scanning tunnelling microscopy (STM), temperature programmed desorption (TPD) spectroscopy and initial catalytic studies for further understanding of the SAA

In order to understand this effect further the authors undertook desorption measurements and high resolution STM (again under UHV conditions).⁵⁰ STM imaging indicated the presence of individual palladium atoms on the copper surface. These isolated palladium atoms were seen to lower the energy barriers for both hydrogen uptake and desorption from the copper surface, with depressions seen in the STM imaging due to the low electron

tunnelling probability calculated.^{55,56} The facile dissociation of hydrogen on palladium in combination with the weak binding to the copper surface allowed for very selective hydrogenation of styrene and acetylene.

The catalytic behaviour of the SAA was then evaluated. The adsorption and desorption of hydrogen for the low temperature selective catalytic hydrogenation of styrene and acetylene was focused upon. Styrene was of interest due to its strong binding *via* π interactions to copper. This strong binding makes copper inactive as a catalyst for styrene hydrogenation. Acetylene was chosen as its selective conversion to ethylene is an industrially important reaction. This reaction has been studied extensively for Pd(111) and Cu(111),^{57,58} allowing for ready comparison. For the hydrogenation of styrene it was found that ethylbenzene was the only product seen. A conversion of 13% and a selectivity of over 95% was detected, as determined by mass spectrometry. Furthermore, no decomposition products of styrene were seen. It was therefore concluded that single palladium atoms had converted the otherwise inactive Cu(111) surface into a highly selective hydrogenation catalyst. TPR analysis also showed the adsorption of unreacted styrene. This was believed to be an indication that the addition of small amounts of palladium had not altered the adsorption properties of the molecule. For acetylene hydrogenation the catalyst was seen to be highly selective. Two reaction routes were established, for high and low reaction temperatures. The high temperature route was assigned to the decomposition and self-hydrogenation of acetylene. SAAs comprised of small quantities of individual and isolated atoms of a catalytically active metal such as palladium significantly impacted the catalytic properties of the less reactive host metal (in this case copper).

6.2.1.3. Development of the SAA strategy for the synthesis of a heterogeneous hydrogenation catalyst for use under more realistic operating conditions

Later work by the group expanded upon the SAA strategy,⁵⁹ to allow for the systematic design and preparation of a supported heterogeneous catalyst that could work under ambient rather than vacuum conditions. This catalyst was used for selective hydrogenation. Synthesis of this SAA took place using galvanic replacement (GR) to incorporate palladium atoms onto the surface of pre-formed conventional copper catalysts. The palladium concentration was kept low (copper to palladium atomic ratio 83:1) with the goal of avoiding palladium islands forming, which it was thought could lead to poor catalyst selectivity (as observed on pure palladium). The catalytic performance of this material was then tested for the partial hydrogenation of phenylacetylene. Significant enhancements in the catalysts activity and selectivity were seen. The activity was seen to increase by an order of magnitude

as compared to the traditional monometallic copper catalyst and the selectivity to styrene was greater than 94%.

6.2.1.4. Synthesis of copper-platinum SAA type catalysts by GR

Finally, this methodology has been reported with other suitable noble metals such as platinum. Lucci *et al.*,⁶⁰ prepared a copper and platinum SAA for the hydrogenation of 1,3-butadiene, using adaptation of the GR method reported by Kyriakou *et al.*.⁵⁸ The SAA synthesised had a ratio of 1 platinum atom per 100 copper atoms and displayed high activity and enhanced selectivity for the hydrogenation of 1,3-butadiene even under mild conditions. In accordance with the theory outlined above (of the precious metal facilitating hydrogen dissociation and spillover onto the copper surface) isolated platinum atoms were seen by STM imaging, and TPD spectroscopy showed a reduction in the temperature at which hydrogen desorption was seen compared to the monometallic platinum catalyst. This indicated that copper-platinum SAA materials could work on an analogous basis to the platinum ones. The work within this report focuses upon fabricating copper-platinum SAAs for the selective hydrogenation of furfural. The target of furfural was that this SAA methodology would also work for an important biomass transformation (good catalysts are already available for the transformation studied above, and as described this is not the case for this reaction). Also, unlike these previous reports, the use of nanoparticle materials synthesised within this thesis will allow the GR step to be performed on the nanoparticle not a supported catalyst. Achieving this both facilitates use of other characterisation techniques, such as high resolution (HR)-TEM and aberration corrected (AC)-TEM, which is easier on the unsupported particle and furthermore allows phenomena such as support effects to be studied in isolation from the SAA synthesis. This section details the synthesis, characterisation, and subsequent catalytic testing under realistic temperatures and pressures (*i.e.* not UHV) of platinum₁copper₈₃ SAAs.

6.2.2. Characterisation of copper nanoparticles with small amounts of platinum

6.2.2.1. TEM imaging of supported and un-supported platinum and copper Single Atom Alloys (SAAs)

Platinum₁copper₈₃ SAA nanoparticles were synthesised *via* addition of a platinum salt (platinum(II) acetylacetonate) into as synthesised metallic copper nanoparticles before exposure to air. Unincorporated platinum and displaced copper were removed by subsequent washing (see Section 2.2.1.7). TEM imaging indicated particles displayed a similar size distribution to those synthesised by the analogous copper preparation (Figure 6.9 A, B). No significant changes in particle shape or appearance were seen. It should be

noted that particle size was measured specific to one fixed orientation in order to randomise any geometric effects. Determination of whether platinum had been successfully incorporated was not possible using EDX spectroscopy or TEM imaging given the extremely small quantities of platinum used and the imaging resolution possible, although future experiments are planned using national microscopy facilities when available. High-angle annular dark-field scanning transmission electron microscopy (HAADF-STEM) was also trialled but could not resolve the individual atoms of platinum deposited, again due to the small quantity of palladium in the sample. Inductively coupled plasma-optical emission spectrometry (ICP-OES) analysis was therefore used to provide evidence of incorporation of the platinum into the copper nanoparticles.

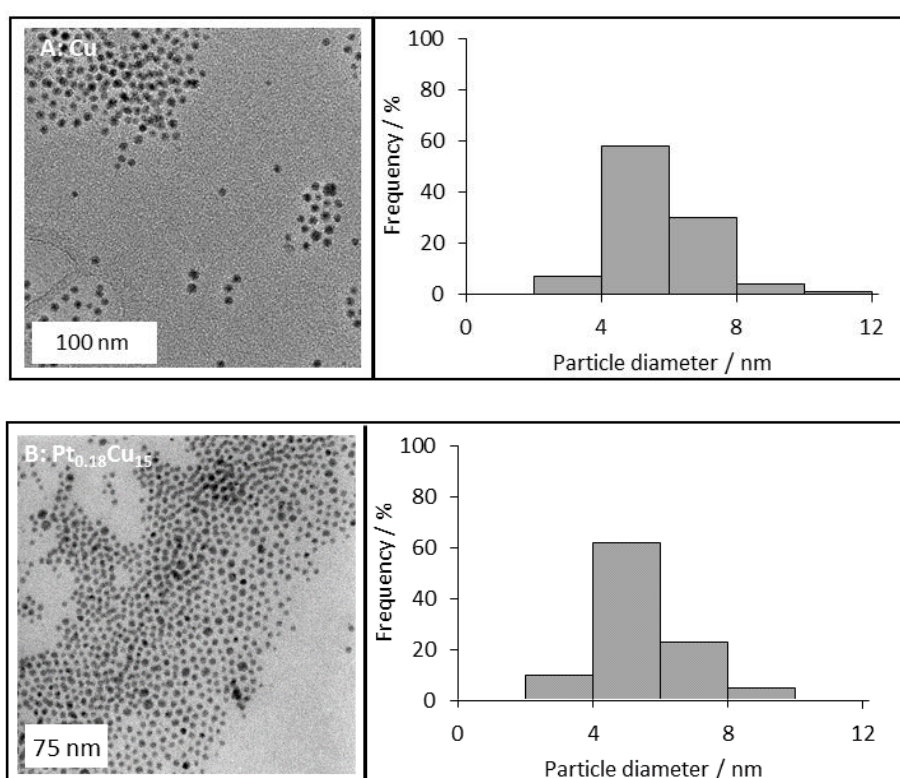


Figure 6.9. A) (left) Typical TEM image of as synthesised copper/octadecylamine nanoparticles (copper/ODA nps) synthesised with 0.46 mmol morpholine borane complex (prepared as outlined in Section 2.2.1.5), (right) corresponding particle size distribution of 6 ± 1 nm, obtained from multiple images of this sample. B) (left) Typical TEM image of as synthesised platinum₁copper₈₃/octadecylamine nanoparticles (platinum₁copper₈₃/ODA nps) synthesised with 0.46 mmol morpholine borane complex (prepared as outlined in Section 2.2.1.7), (right) corresponding particle size distribution of 5 ± 1 nm obtained from multiple images of this sample.

6.2.2.2. ICP-OES analysis of platinum and copper Single Atom Alloys (SAAs)

6.2.2.2.1. ICP-OES for platinum₁copper₈₃ nanoparticles

Results of digestion and elemental analysis using ICP-OES for unsupported platinum₁copper₈₃ nanoparticles are given in Table 6.6. Upon following the typical procedure for analysis by ICP-

OES in which removal of the solvent (hexane) by gentle heating under a flow of nitrogen is followed by the addition of and heating with aqua regia (at 80 °C for 1 h), some inhomogeneity was seen in the cooled sample. Correspondingly two differing digestion methods (using nitric acid and hydrochloric acid) were trialled. Results (Table 6.6) showed that for the unsupported nanoparticles aqua regia gave the highest and most comparable metal conversions for both platinum and copper indicating a conversion of 59 and 53% respectively. This indicated the successful incorporation of platinum in the as synthesised platinum₁copper₈₃ nanoparticles. Aqua regia was, therefore, chosen as the digestion medium for this analysis of the platinum₁copper₈₃ SAA nanoparticles by ICP-OES. In order to allow for catalytic testing, both pure copper and platinum₁copper₈₃ nanoparticles were supported by an identical method on alumina. The two catalysts were prepared, using incipient wetness techniques (see Section 2.2.3.3), with an intended metal loading of 1 and 2 wt.% for the monometallic and bimetallic materials respectively. The nanoparticles were supported upon alumina in such a way that all the metal should have been incorporated. Therefore, the ICP-OES values given above for the nanoparticles should represent the amount of metal present within the supported catalysts. ICP-OES analysis was attempted for the supported nanoparticles in the presence of alumina but was not successful (potentially hydrogen fluoride digestion could be used to assess this, but was not available, and given the preparation method it was believed the metal content could accurately be calculated from the nanoparticle solution concentration).

Table 6.6. ICP-OES results from three differing digestion methods for platinum₁copper₃₃ unsupported nanoparticles. Concentrations calculated from the copper (Cu) 325nm line and from averaging of results from the platinum (Pt) 214 nm, and 266 nm lines. Errors are derived from standard deviation in the calibration.

Digestion method	Nominal concentration of Pt based on synthesis/ mg mL⁻¹	Nominal concentration of Cu based on synthesis / mg mL⁻¹	Actual Concentration and standard deviation of Pt (from ICP) / mg mL⁻¹	Actual Concentration and standard deviation of Cu (from ICP) / mg mL⁻¹	Cu conversion / %	Pt conversion / %
Aqua regia	1	64	0.587 ± 0.005	34.0 ± 0.1	53.2 ± 0.2	58.7 ± 0.5
Nitric acid	1	64	0.147 ± 0.001	35.6 ± 0.2	55.6 ± 0.3	14.7 ± 0.1
Hydrochloric acid	1	64	0.297 ± 0.001	35.8 ± 0.4	56.0 ± 0.6	29.7 ± 0.1

6.2.2.3. Catalytic testing of supported platinum and copper Single Atom Alloys (SAAs)

Catalytic testing of the supported copper/alumina and platinum₁copper₈₃/alumina catalyst was performed by collaborators at Aston University. Results (Figure 6.10), showed the activity of the platinum₁copper₈₃/alumina catalyst was significantly higher than for copper. The activity was almost an order of magnitude higher noting that the total metal loading of the two catalysts was 2:1 for copper: platinum₁copper₈₃. This enhancement suggests that this procedure (*i.e.* the use of GR to prepare a copper catalyst doped with atomic quantities of platinum) can be expanded to also provide enhancements in product conversion for furfural hydrogenation reactions. Importantly it also demonstrates for the first time that the displacement method can be used on unsupported copper nanoparticles, allowing the preparation of single atom alloy catalysts independently of support materials. This might for instance be especially valuable in exploring support or hydrogen spillover effects, where extension of the present work will allow the same single atom alloy nanoparticle sample to be deposited on multiple supports. It should be noted that an induction period was seen. The cause of the induction period remains a topic of future investigation, but was seen with a number of other catalysts in the same testing setup and possible explanations for this induction time include this being time required for the copper catalyst to fully reduce (although pre-reduction does take place prior to catalysis, partial oxidation as a result of handling may occur before reaction), or it is possible that slow removal of the organic capping agent upon the nanoparticle could take place during the induction period. It has been noted previously within this report that capping agents have been thought to prohibit catalytic behaviour,⁶¹ and attempts to remove them had not been made in this study.

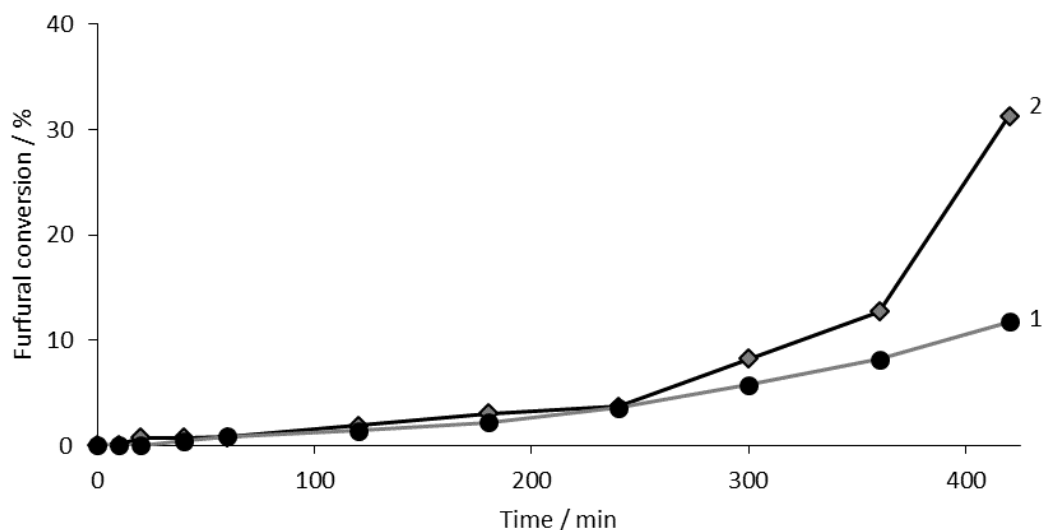


Figure 6.10. Catalytic data (Section 2.2.6.3) showing furfural conversion against catalyst time on-line for 1- copper/alumina (2 wt.% metal) and 2- platinum₁copper₈₃/alumina (1 wt.% metal). Both catalysts had been pre-reduced.

6.3. Palladium nanoparticles for use in hierarchical structured materials

Hierarchically structured materials are of particular interest to a variety of catalytic transformations (such as biofuel synthesis and biomass conversion),⁶² providing the ability to incorporate different chemical functionality into a porous architecture. As part of collaboration with Aston and Leeds University spatially orthogonal bifunctional porous catalysts were synthesised and studied for use in catalytic cascade reactions.⁶³ One key consideration in facilitating this work was the synthesis of a suitably interconnected porous support network. For such micropore-mesopore systems pore diffusion is often low due to the presence of isolated parallel channels, even in cases where the pore properties have been carefully tuned.⁶² This can result in a lowering in the product yield. In order to overcome this diffusion limitation for a SBA-15 mesoporous support, Dhainaut *et al.* synthesised materials with an interconnected mesoporous macroporous structure.⁶² This pore interconnectivity helps to overcome these mass transport limitations.^{64–66} This was achieved using a dual-templating method making use of polystyrene beads and liquid crystalline surfactants, with this method chosen in order to allow for control over the properties of the macropore.^{67–69} Functionalisation of this system with propylsulfonic acid gave rise to the final catalyst with an organised mesoporous-macroporous structure. Enhanced catalytic properties were seen for two reactions in which pore diffusion was key, namely the transesterification of bulky groups (glyceryl trioctanoate), and esterification of a long chain moiety (palmitic acid). In the present work, this interconnected porous network is developed one stage further by putting different catalysts (palladium and platinum) in each pore

channel, with diffusion of reactants being much faster into the macropores than the mesopores. In this way the order of reactions in the cascade reaction can be controlled, this is important when unselective reaction pathways can occur by reactants 'seeing' the catalysts in the wrong order. Palladium nanoparticles were prepared in a similar manner to the synthetic strategies used for copper particles reported earlier, and enabled size and hydrophobicity controlled location of the palladium versus platinum in the pore network. This process was achieved *via* the stepwise removal of a template species, in which polar surfactant Pluronic 123 (P123) and nonpolar polystyrene were used for stepwise extraction of the macropores and mesopores, using solvents of differing polarities. This process was followed by the chemical functionalisation of an interconnected silica framework. This allowed for spatial compartmentalisation of two differing catalyst moieties, allowing for direction of the reaction and control over a catalytic cascade reaction in this case the palladium/platinum-catalysed oxidation of cinnamyl alcohol to cinnamic acid. As part of this the synthesis of palladium nanoparticles of specified and tightly controlled particle size was required, so that they were unable to fit within the smaller channels of the mesopores, ensuring they would only be present in the macropores. Furthermore, to allow for subsequent incorporation of aqueous salts of platinum in the mesopores, based on hydrophilic/hydrophobic behaviour, the macropores had to be hydrophobic and it was therefore advantageous to limit synthetic routes for the preparation of the palladium nanoparticles to ones in which a hydrophobic capping agent was employed. TEM imaging and the corresponding catalytic data from use of these particles in catalysis (as described above) are given within this section. To meet these requirements a synthesis based on that of Mazumder and Sun for oleylamine capped nanoparticles was modified to employ a readily available borane complex,⁷⁰ and by extending the duration of particle ageing at 90 °C to obtain larger nanoparticles.

6.3.1. TEM of palladium nanoparticles

TEM imaging (Figure 6.11) showed the formation of small, monodisperse particles (6 ± 1 nm). Careful control of particle size was required for this application so that palladium would be deposited exclusively into the macropores of the hierarchical structured support (SBA-15). It should be noted that particle size was measured specific to one fixed orientation in order to randomise any geometric effects.

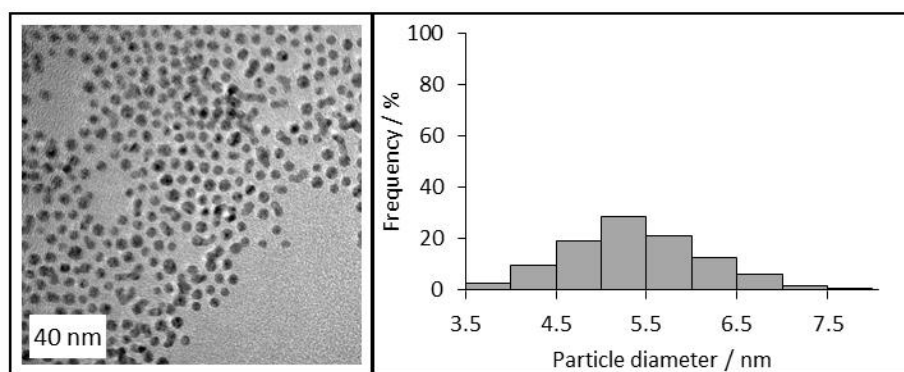


Figure 6.11. A) (left) Typical TEM image of as synthesised palladium/oleylamine nanoparticles (palladium/OAm nanoparticles, prepared as outlined in Section 2.2.1.8), (right) corresponding particle size distribution 6 ± 1 nm) obtained from multiple images of this sample.

6.3.2. ICP-OES of palladium nanoparticles

ICP-OES results for the palladium nanoparticles are shown in Table 6.7 and give a palladium yield of around 50% based on two repeat syntheses shown in the table.

Table 6.7. ICP-OES results for palladium/OAm nps (Pd/OAm nps). ICP-OES concentrations calculated from the 324 and 340 nm palladium (Pd) lines. Errors are derived from standard deviation in the calibration.

Sample	Nominal concentration of Pd based on synthesis/ mg mL^{-1}	Actual Concentration and standard deviation of Pd (from ICP) / mg mL^{-1}	Pd conversion / %
1i)Pd/OAm np	17.4	7.6 ± 0.8	43.5 ± 4.6
1ii)Pd/OAm np	17.4	7.4 ± 0.8	42.8 ± 4.6

6.3.3. Catalytic data from application of palladium nanoparticles

Catalytic testing for the oxidation of cinnamyl alcohol over the hierarchical structured platinum and palladium catalysts supported upon SBA-15 took place at Aston University.⁶³ Catalytic data and comparison of results to literature systems, for which catalysis took place under similar conditions, is given in Table 6.8. Superior (turnover frequencies) TOFs for cinnamic acid are seen along with high selectivity to cinnamyl aldehyde compared to the other literature systems. To the best of our knowledge this is the only heterogeneous catalyst in a one-pot system able to achieve the oxidation of cinnamyl alcohol to the acid in quantifiable yields.

Table 6.8. Comparison of TOF and selectivity data for cinnamyl alcohol oxidation to cinnamyl aldehyde and cinnamic acid for a variety of materials where catalysis took place under broadly similar conditions. Including the use of the base Hydroxyapatite (HAP). For platinum (Pt) and palladium (Pd) hierarchical materials.⁶³ All catalytic testing took place at Aston University.

Catalyst	TOF cinnamyl alcohol conversion / h ⁻¹	Selectivity to cinnamyl aldehyde	TOF cinnamic acid production/ h ⁻¹	Substrate: catalyst molar ratio	Base	Reaction conditions
Hierarchical structured Pt and Pd on SBA-15. ⁶³	8500	71	311	2000	no	150 °C, 5 bar
Pt on SBA-15. ⁷¹	6000	25	0	1500	no	90 °C, 1 bar
Pd on SBA-15. ⁷²	5000	59	0	430_17872	no	90 °C, 1 bar
Pd on Al ₂ O ₃ . ⁷³	400	60	0	6	no	80 °C, 150 bar CO ₂
Pd on CeO ₂ . ⁷⁴	83	99	0	125	no	80 °C, 1 bar
Au-Pd on TiO ₂ . ⁷⁵	97	100	0	5000	no	90 °C, 1 bar
Au-Ag nanotubes. ⁷⁶	800	21.1	0	2000	no	100 °C, 6 bar
Cu on cellulose. ⁷⁷	20	83	0	5	no	100 °C, autogenous
Pd on SBA-16. ⁷⁸	4	99	0	100	K ₂ CO ₃	100 °C, 1 bar
Pd on HAP. ⁷⁹	455	95	0	500	HAP	90 °C, 1 bar
N-doped activated carbon. ⁸⁰	0.18	100	0	2.7	CH ₃ CN	80 °C, 1 bar

6.4. Conclusions

Examples are given within this section showing the use and applicability of nanoparticles prepared using the approach in this thesis, and developed specifically for copper in Chapter 4. In all cases controlled particle size and the ability to independently manipulate the nanoparticle size and/or composition independently of the support have been underpinning attributes that enabled a variety of heterogeneous catalytic applications to be explored. Specifically:

- 1) Silver catalysed amide bond formation was explored based on a literature precedent and although this is discussed more in future work, the use of nanoparticles allowed a previous hypothesis about support effects to be dismissed, because the deposition of the same nanoparticles on different supports showed the presence of acid and base sites, both found on alumina, to be unimportant. Additionally a major factor identified was the strong sensitivity to oxidation/reduction of the silver surface, which requires future exploration.
- 2) The copper nanoparticles developed in Chapter 4 were further modified in the colloidal synthesis mixture using a galvanic displacement method to incorporate palladium – carried out for the first time on the nanoparticles rather than the supported catalyst. This enabled the demonstration of the Single Atom Alloy effect for the hydrogenation of furfural.
- 3) Palladium nanoparticles were prepared with the specific attributes needed to develop a hierarchical catalyst in which different metals are preferentially inserted in the small (meso-) and large (macro-) pores of the material to control the order of a cascade reaction. This was in turn demonstrated on this material by sequential oxidation of cinnamyl alcohol to cinnamaldehyde and then cinnamic acid.

The examples given demonstrate the ability to use the nanoparticle materials of the type reported in this thesis to study catalytic reactions and the, often unique, advantages resulting from this approach.

6.5. Bibliography

- (1) Pattabiraman, V. R.; Bode, J. W. Rethinking Amide Bond Synthesis. *Nature* **2011**, *480* (7378), 471–479.
- (2) Valeur, E.; Bradley, M. Amide Bond Formation: Beyond the Myth of Coupling Reagents. *Chem Soc Rev* **2009**, *38* (2), 606–631.
- (3) Larock, R. C. *Comprehensive Organic Transformations, Two Volume Set*, 2 edition.; Wiley-VCH, 1999.
- (4) Smith, M. B. *Compendium of Organic Synthetic Methods; Compendium of Organic Synthetic Methods*; John Wiley & Sons, Inc.: New York, USA, 2000; Vol. 9.
- (5) Cogley, C. J.; van den Heuvel, M.; Abbadi, A.; de Vries, J. G. Platinum Catalysed Hydrolytic Amidation of Unactivated Nitriles. *Tetrahedron Lett.* **2000**, *41* (14), 2467–2470.
- (6) Owston, N. A.; Parker, A. J.; Williams, J. M. J. Highly Efficient Ruthenium-Catalyzed Oxime to Amide Rearrangement. *Org. Lett.* **2007**, *9* (18), 3599–3601.
- (7) Murahashi, S. I.; Imada, Y.; Nishimura, K. Palladium-Catalyzed Carbonylation of Allylamines. Synthesis of β,γ -Unsaturated Amides by One-Carbon Homologation of Allylamines. *Tetrahedron* **1994**, *50* (2), 453–464.
- (8) Cho, S. H.; Yoo, E. J.; Bae, I.; Chang, S. Copper-Catalyzed Hydrative Amide Synthesis with Terminal Alkyne, Sulfonyl Azide, and Water. *J. Am. Chem. Soc.* **2005**, *127* (46), 16046–16047.
- (9) Gunanathan, C.; Ben-David, Y.; Milstein, D. Direct Synthesis of Amides from Alcohols and Amines with Liberation of H_2 . *Science* **2007**, *317* (5839), 790–792.
- (10) Chan, W. K.; Ho, C. M.; Wong, M. K.; Che, C. M. Oxidative Amide Synthesis and N-Terminal α -Amino Group Ligation of Peptides in Aqueous Medium. *J. Am. Chem. Soc.* **2006**, *128* (46), 14796–14797.
- (11) Zhang, J.; Leitus, G.; Ben-David, Y.; Milstein, D. Facile Conversion of Alcohols into Esters and Dihydrogen Catalyzed by New Ruthenium Complexes. *J. Am. Chem. Soc.* **2005**, *127* (31), 10840–10841.
- (12) Zhang, J.; Leitus, G.; Ben-David, Y.; Milstein, D. Efficient Homogeneous Catalytic Hydrogenation of Esters to Alcohols. *Angew. Chem. Int. Ed.* **2006**, *45* (7), 1113–1115.
- (13) Ben-Ari, E.; Leitus, G.; Shimon, L. J. W.; Milstein, D. Metal–Ligand Cooperation in C–H and H_2 Activation by an Electron-Rich PNP Ir(I) System: Facile Ligand Dearomatization–Aromatization as Key Steps. *J. Am. Chem. Soc.* **2006**, *128* (48), 15390–15391.

- (14) Cho, C. S.; Kim, B. T.; Kim, T. J.; Shim, S. C. An Unusual Type of Ruthenium-Catalyzed Transfer Hydrogenation of Ketones with Alcohols Accompanied by C- C Coupling. *J. Org. Chem.* **2001**, *66* (26), 9020–9022.
- (15) Taguchi, K.; Nakagawa, H.; Hirabayashi, T.; Sakaguchi, S.; Ishii, Y. An Efficient Direct α -Alkylation of Ketones with Primary Alcohols Catalyzed by $[\text{Ir}(\text{cod})\text{Cl}]_2 / \text{PPh}_3 / \text{KOH}$ System without Solvent. *J. Am. Chem. Soc.* **2004**, *126* (1), 72–73.
- (16) Cho, C. A Palladium-Catalyzed Route for α -Alkylation of Ketones by Primary Alcohols. *J. Mol. Catal. Chem.* **2005**.
- (17) Cho, C. S.; Kim, J. H.; Kim, T. J.; Shim, S. C. Ruthenium-Catalyzed Heteroannulation of Anilines with Alkanolammonium Chlorides Leading to Indoles. *Tetrahedron* **2001**, *57* (16), 3321–3329.
- (18) Fujita, K.; Yamamoto, K.; Yamaguchi, R. Oxidative Cyclization of Amino Alcohols Catalyzed by a Cp^*Ir Complex. Synthesis of Indoles, 1,2,3,4-Tetrahydroquinolines, and 2,3,4,5-Tetrahydro-1-Benzazepine. *Org. Lett.* **2002**, *4* (16), 2691–2694.
- (19) Matsu-ura, T.; Sakaguchi, S.; Obora, Y.; Ishii, Y. Guerbet Reaction of Primary Alcohols Leading to β -Alkylated Dimer Alcohols Catalyzed by Iridium Complexes. *J. Org. Chem.* **2006**, *71* (21), 8306–8308.
- (20) Shimizu, K.; Ohshima, K.; Satsuma, A. Direct Dehydrogenative Amide Synthesis from Alcohols and Amines Catalyzed by γ -Alumina Supported Silver Cluster. *Chem. Eur. J.* **2009**, *15* (39), 9977–9980.
- (21) Valden, M. Onset of Catalytic Activity of Gold Clusters on Titania with the Appearance of Nonmetallic Properties. *Science* **1998**, *281* (5383), 1647–1650.
- (22) Haruta, M. Gold Catalysts Prepared by Coprecipitation for Low-Temperature Oxidation of Hydrogen and of Carbon Monoxide. *J. Catal.* **1989**, *115* (2), 301–309.
- (23) Bell, A. T. The Impact of Nanoscience on Heterogeneous Catalysis. *Science* **2003**, *299* (5613), 1688–1691.
- (24) Rolison, D. R. Catalytic Nanoarchitectures—the Importance of Nothing and the Unimportance of Periodicity. *Science* **2003**, *299* (5613), 1698–1701.
- (25) Shimizu, K.; Sugino, K.; Sawabe, K.; Satsuma, A. Oxidant-Free Dehydrogenation of Alcohols Heterogeneously Catalyzed by Cooperation of Silver Clusters and Acid-Base Sites on Alumina. *Chem. - Eur. J.* **2009**, *15* (10), 2341–2351.
- (26) Sun, T.; Seff, K. Silver Clusters and Chemistry in Zeolites. *Chem. Rev.* **1994**, *94* (4), 857–870.
- (27) Dr G. Kyriakou. Aston University Private Communication.

- (28) Fu, Q.; Wagner, T. Interaction of Nanostructured Metal Overlayers with Oxide Surfaces. *Surf. Sci. Rep.* **2007**, *62* (11), 431–498.
- (29) Koski, K. J.; Kamp, N. M.; Smith, R. K.; Kunz, M.; Knight, J. K.; Alivisatos, A. P. Structural Distortions in 5–10 Nm Silver Nanoparticles under High Pressure. *Phys. Rev. B* **August 10**, *78* (16), 165410.
- (30) Reddy, B. M.; Reddy, G. K.; Rao, K. N.; Khan, A.; Ganesh, I. Silica Supported Transition Metal-Based Bimetallic Catalysts for Vapour Phase Selective Hydrogenation of Furfuraldehyde. *J. Mol. Catal. Chem.* **2007**, *265* (1–2), 276–282.
- (31) Corma, A.; Iborra, S.; Velty, A. Chemical Routes for the Transformation of Biomass into Chemicals. *Chem. Rev.* **2007**, *107* (6), 2411–2502.
- (32) Nagaraja, B. M.; Padmasri, A. H.; David Raju, B.; Rama Rao, K. S. Vapor Phase Selective Hydrogenation of Furfural to Furfuryl Alcohol over Cu–MgO Coprecipitated Catalysts. *J. Mol. Catal. Chem.* **2007**, *265* (1–2), 90–97.
- (33) Rao, R.; Dandekar, A.; Baker, R. T. K.; Vannice, M. A. Properties of Copper Chromite Catalysts in Hydrogenation Reactions. *J. Catal.* **1997**, *171* (2), 406–419.
- (34) Rao, R. S.; Baker, R. T. K.; Vannice, M. A. Furfural Hydrogenation over Carbon-supported Copper. *Catal. Lett.* **1999**, *60* (1–2), 51–57.
- (35) Egeblad, K.; Rass-Hansen, J.; Marsden, C. C.; Taarning, E.; Christensen, C. H. Heterogeneous Catalysis for Production of Value-Added Chemicals from Biomass. *Catalysis* **2009**, *21*, 13–50.
- (36) Gowda, A. S.; Parkin, S.; Ladipo, F. T. Hydrogenation and Hydrogenolysis of Furfural and Furfuryl Alcohol Catalyzed by ruthenium(II) Bis(diimine) Complexes. *Appl. Organomet. Chem.* **2012**, *26* (2), 86–93.
- (37) Nakagawa, Y.; Nakazawa, H.; Watanabe, H.; Tomishige, K. Total Hydrogenation of Furfural over a Silica-Supported Nickel Catalyst Prepared by the Reduction of a Nickel Nitrate Precursor. *ChemCatChem* **2012**, *4* (11), 1791–1797.
- (38) Panagiotopoulou, P.; Vlachos, D. G. Liquid Phase Catalytic Transfer Hydrogenation of Furfural over a Ru/C Catalyst. *Appl. Catal. Gen.* **2014**, *480*, 17–24.
- (39) Kijeński, J.; Winiarek, P.; Paryjczak, T.; Lewicki, A.; Mikołajska, A. Platinum Deposited on Monolayer Supports in Selective Hydrogenation of Furfural to Furfuryl Alcohol. *Appl. Catal. Gen.* **2002**, *233* (1–2), 171–182.
- (40) Luo, H.; Li, H.; Zhuang, L. Furfural Hydrogenation to Furfuryl Alcohol over a Novel Ni–Co–B Amorphous Alloy Catalyst. *Chem. Lett.* **2001**, *30* (5), 404–405.

- (41) Pushkarev, V. V.; Musselwhite, N.; An, K.; Alayoglu, S.; Somorjai, G. A. High Structure Sensitivity of Vapor-Phase Furfural Decarbonylation/Hydrogenation Reaction Network as a Function of Size and Shape of Pt Nanoparticles. *Nano Lett.* **2012**, *12* (10), 5196–5201.
- (42) Baker, L. R.; Kennedy, G.; Van Spronsen, M.; Hervier, A.; Cai, X.; Chen, S.; Wang, L. W.; Somorjai, G. A. Furfuraldehyde Hydrogenation on Titanium Oxide-Supported Platinum Nanoparticles Studied by Sum Frequency Generation Vibrational Spectroscopy: Acid–Base Catalysis Explains the Molecular Origin of Strong Metal–Support Interactions. *J. Am. Chem. Soc.* **2012**, *134* (34), 14208–14216.
- (43) An, K.; Musselwhite, N.; Kennedy, G.; Pushkarev, V. V.; Robert Baker, L.; Somorjai, G. A. Preparation of Mesoporous Oxides and Their Support Effects on Pt Nanoparticle Catalysts in Catalytic Hydrogenation of Furfural. *J. Colloid Interface Sci.* **2013**, *392*, 122–128.
- (44) Sitthisa, S.; Pham, T.; Prasomsri, T.; Sooknoi, T.; Mallinson, R. G.; Resasco, D. E. Conversion of Furfural and 2-Methylpentanal on Pd/SiO₂ and Pd–Cu/SiO₂ Catalysts. *J. Catal.* **2011**, *280* (1), 17–27.
- (45) Sitthisa, S.; An, W.; Resasco, D. E. Selective Conversion of Furfural to Methylfuran over Silica-Supported Ni Fe Bimetallic Catalysts. *J. Catal.* **2011**, *284* (1), 90–101.
- (46) Taylor, M. J.; Jiang, L.; Reichert, J.; Papageorgiou, A. C.; Beaumont, S. K.; Wilson, K.; Lee, A. F.; Barth, J. V.; Kyriakou, G. Catalytic Hydrogenation and Hydrodeoxygenation of Furfural over Pt(111): A Model System for the Rational Design and Operation of Practical Biomass Conversion Catalysts. *J. Phys. Chem. C* **2017**, *121* (15), 8490–8497.
- (47) Tierney, H. L.; Baber, A. E.; Kitchin, J. R.; Sykes, E. C. H. Hydrogen Dissociation and Spillover on Individual Isolated Palladium Atoms. *Phys. Rev. Lett.* **2009**, *103* (24).
- (48) Tierney, H. L.; Baber, A. E.; Sykes, E. C. H. Atomic-Scale Imaging and Electronic Structure Determination of Catalytic Sites on Pd/Cu Near Surface Alloys. *J. Phys. Chem. C* **2009**, *113* (17), 7246–7250.
- (49) Bellisario, D. O.; Han, J. W.; Tierney, H. L.; Baber, A. E.; Sholl, D. S.; Sykes, E. C. H. Importance of Kinetics in Surface Alloying: A Comparison of the Diffusion Pathways of Pd and Ag Atoms on Cu(111). *J. Phys. Chem. C* **2009**, *113* (29), 12863–12869.
- (50) Kyriakou, G.; Boucher, M. B.; Jewell, A. D.; Lewis, E. A.; Lawton, T. J.; Baber, A. E.; Tierney, H. L.; Flytzani-Stephanopoulos, M.; Sykes, E. C. H.; others. Isolated Metal Atom Geometries as a Strategy for Selective Heterogeneous Hydrogenations. *Sci. Wash.* **2012**, *335* (6073), 1209–1212.

- (51) Gutés, A.; Carraro, C.; Maboudian, R. Silver Dendrites from Galvanic Displacement on Commercial Aluminum Foil As an Effective SERS Substrate. *J. Am. Chem. Soc.* **2010**, *132* (5), 1476–1477.
- (52) *CRC Handbook of Chemistry and Physics, 95th Edition*, 95 edition.; Haynes, W. M., Ed.; CRC Press: Boca Raton; London; New York, 2014.
- (53) Chopra, I. S.; Chaudhuri, S.; Veyan, J. F.; Chabal, Y. J. Turning Aluminium into a Noble-Metal-like Catalyst for Low-Temperature Activation of Molecular Hydrogen. *Nat. Mater.* **2011**, *10* (11), 884–889.
- (54) Wittstock, A.; Zielasek, V.; Biener, J.; Friend, C. M.; Baumer, M. Nanoporous Gold Catalysts for Selective Gas-Phase Oxidative Coupling of Methanol at Low Temperature. *Science* **2010**, *327* (5963), 319–322.
- (55) Lauhon, L. J.; Ho, W. Direct Observation of the Quantum Tunneling of Single Hydrogen Atoms with a Scanning Tunneling Microscope. *Phys. Rev. Lett.* **2000**, *85* (21), 4566–4569.
- (56) Mitsui, T.; Rose, M. K.; Fomin, E.; Ogletree, D. F.; Salmeron, M. Dissociative Hydrogen Adsorption on Palladium Requires Aggregates of Three or More Vacancies. *Nature* **2003**, *422* (6933), 705–707.
- (57) Tysoe, W. T.; Nyberg, G. L.; Lambert, R. M. Low Temperature Catalytic Chemistry of the Pd(111) Surface: Benzene and Ethylene from Acetylene. *J. Chem. Soc. Chem. Commun.* **1983**, No. 11, 623.
- (58) Kyriakou, G.; Kim, J.; Tikhov, M. S.; Macleod, N.; Lambert, R. M. Acetylene Coupling on Cu(111): Formation of Butadiene, Benzene, and Cyclooctatetraene. *J. Phys. Chem. B* **2005**, *109* (21), 10952–10956.
- (59) Boucher, M. B.; Zugic, B.; Cladaras, G.; Kammert, J.; Marcinkowski, M. D.; Lawton, T. J.; Sykes, E. C. H.; Flytzani-Stephanopoulos, M. Single Atom Alloy Surface Analogs in Pd_{0.18}Cu₁₅ Nanoparticles for Selective Hydrogenation Reactions. *Phys. Chem. Chem. Phys.* **2013**, *15* (29), 12187.
- (60) Lucci, F. R.; Liu, J.; Marcinkowski, M. D.; Yang, M.; Allard, L. F.; Flytzani-Stephanopoulos, M.; Sykes, E. C. H. Selective Hydrogenation of 1,3-Butadiene on Platinum–copper Alloys at the Single-Atom Limit. *Nat. Commun.* **2015**, *6*, 8550.
- (61) Kuhn, J. N.; Tsung, C. K.; Huang, W.; Somorjai, G. A. Effect of Organic Capping Layers over Monodisperse Platinum Nanoparticles upon Activity for Ethylene Hydrogenation and Carbon Monoxide Oxidation. *J. Catal.* **2009**, *265* (2), 209–215.

- (62) Dhainaut, J.; Dacquin, J. P.; Lee, A. F.; Wilson, K. Hierarchical Macroporous–mesoporous SBA-15 Sulfonic Acid Catalysts for Biodiesel Synthesis. *Green Chem* **2010**, *12* (2), 296–303.
- (63) Parlett, C. M. A.; Isaacs, M. A.; Beaumont, S. K.; Bingham, L. M.; Hondow, N. S.; Wilson, K.; Lee, A. F. Spatially Orthogonal Chemical Functionalization of a Hierarchical Pore Network for Catalytic Cascade Reactions. *Nat. Mater.* **2015**, *15* (2), 178–182.
- (64) Imhof, A.; Pine, D. J. Ordered Macroporous Materials by Emulsion Templating. *Nature* **1997**, *389* (6654), 948–951.
- (65) Deng, W.; Toepke, M. W.; Shanks, B. H. Surfactant-Assisted Synthesis of Alumina with Hierarchical Nanopores. *Adv. Funct. Mater.* **2003**, *13* (1), 61–65.
- (66) Yuan, Z. Y.; Su, B. L. Insights into Hierarchically Meso–macroporous Structured Materials. *J Mater Chem* **2006**, *16* (7), 663–677.
- (67) Yun, J. S.; Ihm, S. K. Synthesis of Mesoporous SBA-15 Having Macropores by Dual-Templating Method. *J. Phys. Chem. Solids* **2008**, *69* (5–6), 1133–1135.
- (68) Oh, C. G.; Baek, Y.; Ihm, S. K. Synthesis of Skeletal-Structured Biporous Silicate Powders through Microcolloidal Crystal Templating. *Adv. Mater.* **2005**, *17* (3), 270–273.
- (69) Sen, T.; Tiddy, G. J. T.; Casci, J. L.; Anderson, M. W. Synthesis and Characterization of Hierarchically Ordered Porous Silica Materials. *Chem. Mater.* **2004**, *16* (11), 2044–2054.
- (70) Mazumder, V.; Sun, S. Oleylamine-Mediated Synthesis of Pd Nanoparticles for Catalytic Formic Acid Oxidation. *J. Am. Chem. Soc.* **2009**, *131* (13), 4588–4589.
- (71) Durndell, L. J.; Parlett, C. M. A.; Hondow, N. S.; Wilson, K.; Lee, A. F. Tunable Pt Nanocatalysts for the Aerobic Selo_x of Cinnamyl Alcohol. *Nanoscale* **2013**, *5* (12), 5412.
- (72) Parlett, C. M. A.; Bruce, D. W.; Hondow, N. S.; Lee, A. F.; Wilson, K. Support-Enhanced Selective Aerobic Alcohol Oxidation over Pd/Mesoporous Silicas. *ACS Catal.* **2011**, *1* (6), 636–640.
- (73) Caravati, M.; Meier, D. M.; Grunwaldt, J. D.; Baiker, A. Continuous Catalytic Oxidation of Solid Alcohols in Supercritical CO₂: A Parametric and Spectroscopic Study of the Transformation of Cinnamyl Alcohol over Pd/Al₂O₃. *J. Catal.* **2006**, *240* (2), 126–136.
- (74) Chen, C.; Fang, X.; Wu, B.; Huang, L.; Zheng, N. A Multi-Yolk-Shell Structured Nanocatalyst Containing Sub-10 Nm Pd Nanoparticles in Porous CeO₂. *ChemCatChem* **2012**, *4* (10), 1578–1586.

- (75) Enache, D. I. Solvent-Free Oxidation of Primary Alcohols to Aldehydes Using Au-Pd/TiO₂ Catalysts. *Science* **2006**, *311* (5759), 362–365.
- (76) Costa, J. C. S.; Corio, P.; Rossi, L. M. Catalytic Oxidation of Cinnamyl Alcohol Using Au–Ag Nanotubes Investigated by Surface-Enhanced Raman Spectroscopy. *Nanoscale* **2015**, *7* (18), 8536–8543.
- (77) Markó, I. E.; Gautier, A.; Dumeunier, R.; Doda, K.; Philippart, F.; Brown, S. M.; Urch, C. J. Efficient, Copper-Catalyzed, Aerobic Oxidation of Primary Alcohols. *Angew. Chem. Int. Ed.* **2004**, *43* (12), 1588–1591.
- (78) Yang, H.; Han, X.; Ma, Z.; Wang, R.; Liu, J.; Ji, X. Palladium-Guanidine Complex Immobilized on SBA-16: A Highly Active and Recyclable Catalyst for Suzuki Coupling and Alcohol Oxidation. *Green Chem.* **2010**, *12* (3), 441.
- (79) Mori, K.; Hara, T.; Mizugaki, T.; Ebitani, K.; Kaneda, K. Hydroxyapatite-Supported Palladium Nanoclusters: A Highly Active Heterogeneous Catalyst for Selective Oxidation of Alcohols by Use of Molecular Oxygen. *J. Am. Chem. Soc.* **2004**, *126* (34), 10657–10666.
- (80) Watanabe, H.; Asano, S.; Fujita, S.; Yoshida, H.; Arai, M. Nitrogen-Doped, Metal-Free Activated Carbon Catalysts for Aerobic Oxidation of Alcohols. *ACS Catal.* **2015**, *5* (5), 2886–2894.